

Effect of Expansion and Magnetic Field Configuration on Mass Entrainment of Jets

A. Rosen ^{a,1}, P.E. Hardee ^{a,2}

^a*University of Alabama, Department of Physics & Astronomy
Tuscaloosa, AL 35487*

Abstract

We investigate the growth of jet plus entrained mass in simulations of supermagnetosonic cylindrical and expanding jets. The entrained mass spatially grows in three stages: from an initially slow spatial rate to a faster rate and finally at a flatter rate. These stages roughly coincide with the similar rates of expansion in simulated radio intensity maps, and also appear related to the growth of the Kelvin-Helmholtz instability through linear, nonlinear, and saturated regimes. In the supermagnetosonic cylindrical jets, we found that a jet with an embedded primarily toroidal magnetic field is more stable than a jet with a primarily axial magnetic field. Also, pressure-matched expanding jets are more stable and entrain less mass than cylindrical jets with equivalent inlet conditions.

1 Motivation

Mass entrainment affects the propagation of jets, and at least one model suggests that its presence may be a distinguishing factor between the two Fanaroff-Riley morphological types of radio galaxies (Bicknell 1994, Bicknell 1996). This work investigates whether there are observable consequences of jets entraining their surrounding medium and also determines the extent of the role that the Kelvin-Helmholtz (or KH) instability has in mass entrainment of magnetized jets. Acceleration and collimation numerical models, e.g., (Lovelace & Romanova 1996, Königl 1989, Pudritz, McLaughlin, & Ouyed 1997) require that a strong magnetic field is associated with the jet near its origin. Jets exit the region near the origin with magnetic fields aligned primarily along the jet axis, i.e. an axial field, or primarily wrapped around the jet axis, i.e. a toroidal or helical field. Observations of extended jets, e.g., 4C 32.69, (Potash & Wardle 1980); M87, (Owen, Hardee, & Cornwell 1989); and NGC 6251,

¹ E-mail: rosen@eclipse.astr.ua.edu

² E-mail: hardee@athena.astr.ua.edu

(Birkinshaw & Worrall 1993) indicate that the jet is overpressured with respect to an external medium and in need of additional confinement that could be provided by magnetic fields. Linear analysis of the KH instability suggests that growth lengths of KH modes are proportional to the product of magnetosonic Mach number and radius (Hardee, Clarke, & Rosen 1997), suggesting that expanding jets are more stable. Here we report on a comparison of supermagnetosonic cylindrical jets and expanding supermagnetosonic jets with roughly equivalent inlet conditions.

2 Some Details of the Simulations

All of these simulations were performed with a version of ZEUS-3D with CMoC (Clarke 1996) that solves the transverse momentum transport and magnetic induction equations simultaneously and in a *planar split* fashion. A second-order accurate MUTCI scheme (van Leer 1977) is used for advection. Two sets of simulations of equilibrium jets have been performed, which simulate a jet and cocoon well behind the bow shock and *not* a jet propagating into an ambient ISM/ICM/IGM.

The set of supermagnetosonic, initially cylindrical jets includes three pairs of simulations, each of which has one simulation with a primarily axial magnetic field and one with a primarily toroidal magnetic field, for dense jets with strong fields, dense jets with weak fields, and light jets strong fields. A complete discussion of these simulations is in Rosen et al. (1999). For the light jets, we set the jet-to-external density ratio, η , equal to 0.25 and for the dense jets, $\eta = 4$. In the comparison set of expanding supermagnetosonic axial field jets, there are three simulations that have conditions at the inlet similar (but not identical) to some of the simulations in the first set. These jets contain primarily axial magnetic fields and the jet radius expands to 1.5 times the inlet jet radius, R_0 , at a position along the jet axis, $z/R_0 = 60$.

The simulations have been completed on a grid that contains some combination of uniform and ratioed zones along each axis. In the uniform portion of the grid, there are 7.5 zones/ R_0 along the jet axis and 15 zones/ R_0 transverse to the jet axis. The boundary conditions for all the simulations are outflow everywhere, except at the jet inlet. The jet is precessed with a small transverse velocity (with an amplitude of $\sim 1\%$ of the axial jet velocity), which breaks the symmetry and should excite the helical modes of the KH instability. In all of the simulations, the precession induces a helical twist in the same sense as that of the magnetic field helicity and helical wavefronts are at shallow angles to the helically twisted magnetic field lines.

3 Results

All figures are shown when the simulation has reached a quasi-steady state out to $z \sim 40\text{--}50R_0$.

3.1 Mass Entrainment

As a proxy for jet plus entrained mass, we compute the linear mass density of magnetized mass. We define the linear mass density, σ , at any point along the jet as $\sigma(z) = \int_A f \rho \, dx dy$, where A is the cross-sectional area of the computational domain at z , and f is a switch set to 1 if the local magnetic field is above a threshold value and $f = 0$ otherwise. We set the threshold to $0.04 B_{max}$, where $B_{max}^2(z)$ is the expected maximum magnetic field in the jet at axial position z . In a steady expanding flow, B_ϕ should vary as $R(z)^{-1}$ and B_z should vary as $R(z)^{-2}$. Since there is some numerical diffusion of the magnetic field not associated with the mixing of jet material and unmagnetized external material, we have found that a threshold based on 4% B_{max} is a useful demarcation between “mixed” (i.e., jet plus entrained material) and “unmixed” regions. In Figure 1, we show the linear mass density normalized to the initial jet value for five dense jet (three cylindrical and two expanding) simulations and three light jet (two cylindrical and one expanding) simulations.

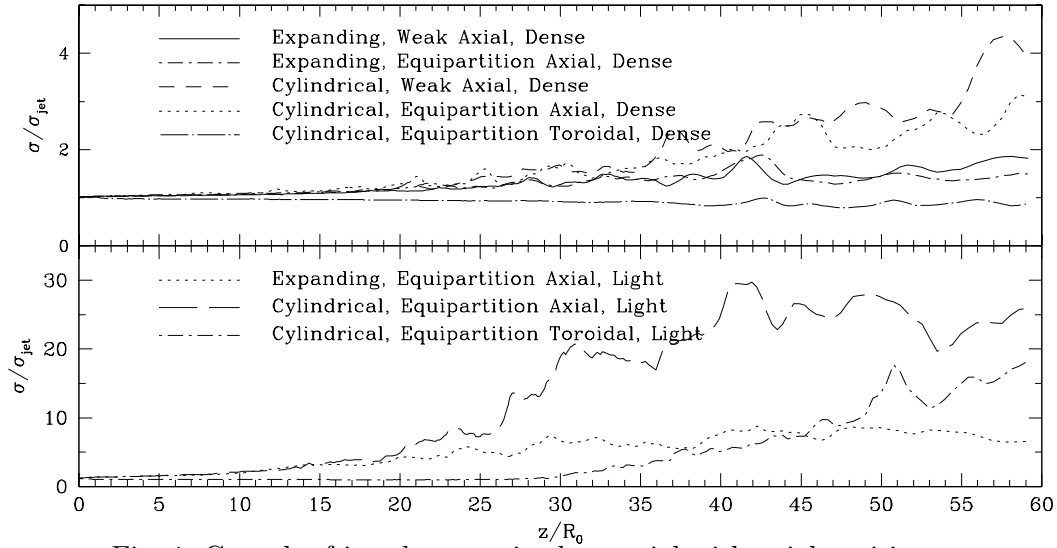


Fig. 1. Growth of jet plus entrained material with axial position.

3.2 Simulated Intensity Maps

In Figure 2, we display maps of simulated radio intensity, which are integrations of $p_{th}(B \sin \theta)^{3/2}$, where θ is the angle between the line-of-sight and the magnetic field, for the dense and light expanding jet simulations with an equipartition axial magnetic field. In order to show the differences in the spine-sheath structure between the simulations, we have used different grayscales in each panel of Figure 2, in which the range covers 3 orders of magnitude and the grayscale maximum is 20% above the actual maximum intensity in each panel. The total intensity is overlaid by B-field polarization vectors that cover regions where the intensity is above 0.001 of the maximum intensity.

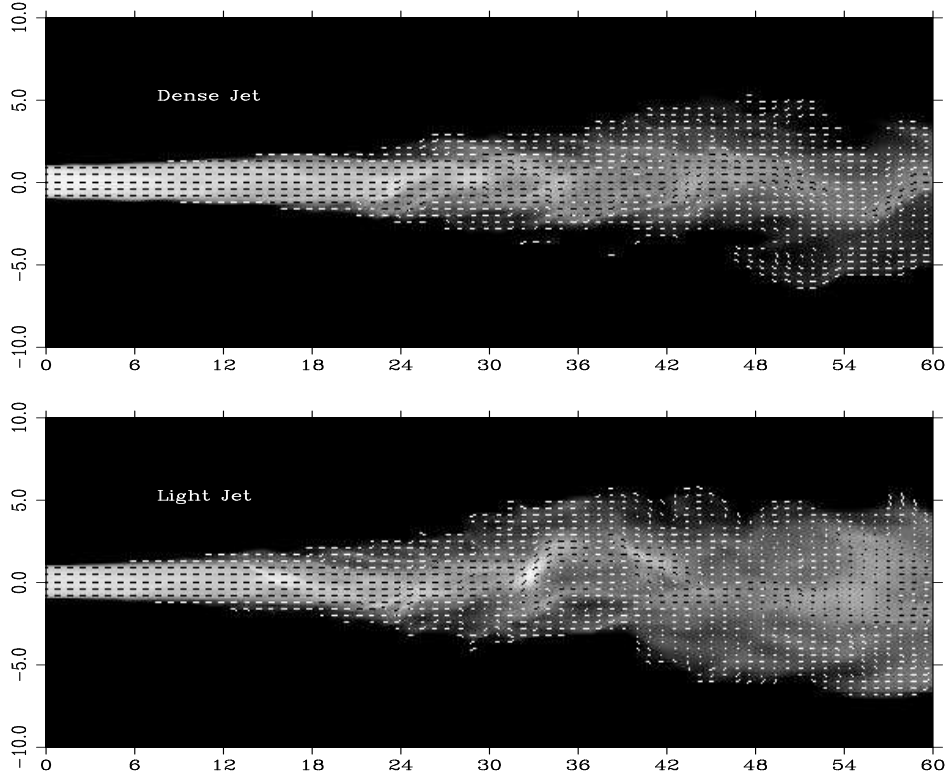


Fig. 2. Simulated intensity maps with B-field polarization vectors overlaid.

3.3 *Example of Structure within Jet*

The growth of the KH instability and its effect on the jet is dramatically demonstrated in the grayscale cross-sections of axial velocity for one simulation (see Figure 3). In this example, the jet surface has many corrugations, which are characteristic of the high order KH fluting modes. In the jet simulations with a primarily axial magnetic field, the KH instability typically progresses from higher order modes with small maximum amplitudes of displacement that dominate close to the inlet to lower order modes with larger distortion amplitudes farther down the jet. An example of these low order modes is the clockwise motion of the jet center about the initial jet axis as one moves down the jet, suggestive of the helical mode. A relatively strong toroidal magnetic field suppresses the growth of the high order modes, although simulations of jets with this magnetic field configuration do show evidence for growth of the (low order) helical mode.

4 Discussion

Spatial growth of magnetized or entrained mass, as measured by the linear mass density, passes through three stages: an initial slowly growing stage with a shallow slope, a stage where the growth rate increases substantially, and a final stage where the linear mass density does not increase. The third stage is most noticeable in the (axial field) light jet simulations, which develop more

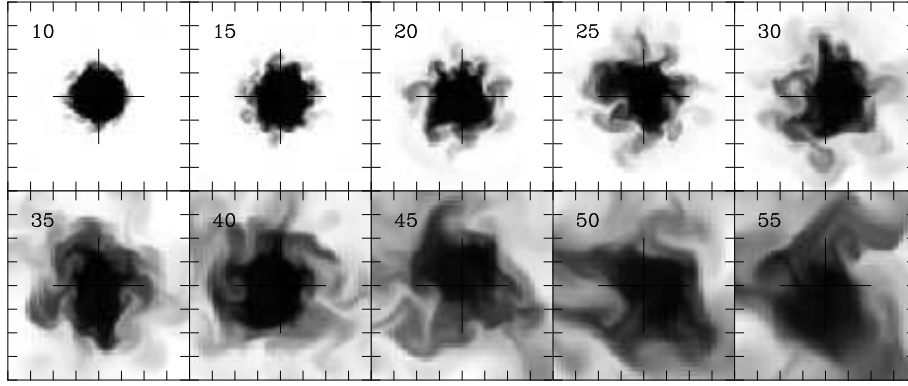


Fig. 3. Grayscale cross-sections of the axial component of velocity for the expanding jet simulation with an equipartition axial magnetic field.

quickly than dense jet simulations. For example, in both axial field simulations in the bottom panel of Figure 1, each stage spans roughly one-third of the simulated jet axis in the light jet with an axial field. In jets with a moderate magnetic field strength, either a primarily toroidal field or jet expansion can reduce the mass entrained by the jet. The expanding jet simulations have an isothermal pressure-matched external medium, which falls off in density. It is this decrease in density that is responsible for the smaller amount of mass entrained in the expanding jet simulations (see the comparison with the cylindrical equivalents in Figure 1). From a comparison of positions where the transitions between regions of slow, fast, and no mass entrainment occur in the different sets of simulations, the expanding supermagnetosonic jets are more stable than their cylindrical equivalents.

From a comparison of our results with predictions from a linear stability analysis (for growth lengths of modes), we confirm that the three stages of growth of the jet plus entrained mass match the stages of growth for the KH instability as it progresses through linear, nonlinear, and saturated stages (Rosen & Hardee 2000). The linear stage is associated with the progression from high order modes to low order modes, the nonlinear with development of large amplitude low order modes and saturation with the maximum amplitude of the low order modes. This progression from high order modes to low order modes is displayed in cross-sections of axial velocity (e.g., Figure 3). By the axial position where the flow is dominated by the elliptical and helical modes, the magnetized “core” of the jet begins to disrupt and is no longer noticeable in the simulated intensity images (e.g., Figure 2). Additionally, the width of the magnetized mass as it appears in simulated intensity images grows in three similar stages. Thus, we do find an observable consequence of mass entrainment. This progression in the expansion of the jets in the intensity images is most noticeable in the light jet simulations, where the region of constant apparent width also has a more uniform intensity than any portion of the dense jets. This uniform appearance suggests a greater mixing of jet and external material in the light jets.

References

- Bicknell, G.V. 1994, *ApJ*, 422, 542.
- Bicknell, G.V. 1996, in *ASP Conf. Ser. 100: Energy Transport in Radio Galaxies and Quasars*, eds. P.E. Hardee, A.H. Bridle, & J.A. Zensus, (San Francisco:ASP) 253.
- Birkinshaw, M., & Worrall, D.M. 1993, *ApJ*, 412, 568.
- Clarke, D.A. 1996, *ApJ*, 457, 291.
- Hardee, P.E., Clarke, D.A., & Rosen, A. 1997, *ApJ*, 485, 533.
- Hardee, P.E., & Rosen, A. 1999, *ApJ*, 524, in press.
- Königl, A. 1989, *ApJ*, 342, 208.
- Lovelace, R.V.E., & Romanova, M.M. 1996, in *ASP Conf. Ser. 100: Energy Transport in Radio Galaxies and Quasars*, ed. P.E. Hardee, A.H. Bridle, & J.A. Zensus, (San Francisco: ASP), 25.
- Owen, F.N., Hardee, P.E., & Cornwell, T.J. 1989, *ApJ*, 340, 698.
- Rosen, A., Hardee, P.E., Clarke, D.A., & Johnson, A. 1999, *ApJ*, 510, 136.
- Rosen, A., & Hardee, P.E. 2000, in preparation.
- Potash, R.I., & Wardle, F.C. 1980, *ApJ*, 239, 42.
- Pudritz, R.E., McLaughlin, D.E., & Ouyed, R. 1997 in *ASP Conf. Ser. 123: The 12th 'Kingston Meeting': Computational Astrophysics*, eds. D.A. Clarke & M.J. West, (San Francisco:ASP) 117.
- van Leer, B. 1977, *J. Comput. Phys.*, 23, 276.